Modelling of classical ghost images obtained using scattered light

2007 New J. Phys. 9 285

(http://iopscience.iop.org/1367-2630/9/8/285)

New Journal of Physics
The open-access journal for physics

Modelling of classical ghost images obtained using scattered light

S Crosby, S Castelletto, C Aruldoss, R E Scholten and A Roberts[1]

School of Physics, University of Melbourne, Victoria, 3010, Australia
E-mail: annr@unimelb.edu.au

New Journal of Physics **9** (2007) 285
Received 8 June 2007
Published 24 August 2007
Online at http://www.njp.org/
doi:10.1088/1367-2630/9/8/285

Abstract. The images obtained in ghost imaging with pseudo-thermal light sources are highly dependent on the spatial coherence properties of the incident light. Pseudo-thermal light is often created by reducing the coherence length of a coherent source by passing it through a turbid mixture of scattering spheres. We describe a model for simulating ghost images obtained with such partially coherent light, using a wave-transport model to calculate the influence of the scattering on initially coherent light. The model is able to predict important properties of the pseudo-thermal source, such as the coherence length and the amplitude of the residual unscattered component of the light which influence the resolution and visibility of the final ghost image. We show that the residual ballistic component introduces an additional background in the reconstructed image, and the spatial resolution obtainable depends on the size of the scattering spheres.

[1] Author to whom any correspondence should be addressed.

PII: S1367-2630(07)52187-7

Contents

1. Introduction

The ghost imaging technique produces an image of an object from a measurement of the fourth-order (i.e. intensity) correlation function. A twin beam configuration is used, in which partially coherent light is split into two paths with the object in one (test) arm (see figure 1). The intensity in that arm is obtained with a detector possessing no spatial resolution. The light in the second (reference) arm is detected with spatial resolution, and the final image is reconstructed from the coincidence between the two detectors. Neither of the detectors independently produces an image of the object, but the correlation between the two permits reconstruction of the image.

Ghost imaging has been demonstrated using twin-beams exhibiting quantum entanglement [1]–[3], and with classically correlated light [4]–[8]. The quantum correlation stems from the information-sharing inherent in any entangled system [9]. Quantum ghost imaging exploits the spatial and momentum correlations between the photons generated in a nonlinear medium, typically in a parametric down-conversion process. It was thought until recently that only a quantum-entangled source could produce the correlations needed to obtain ghost images. It has now been shown that pseudo-thermal light divided by a beam-splitter, producing two classically correlated beams, can replicate nearly all experiments performed using a quantum bi-photon source [6].

Ghost imaging can be performed with photon counting detectors [7], with current measuring detectors such as photodiodes, or with a CCD camera [6]. Image visibility (signal-to-noise ratio) is generally superior with quantum fields and single photon detectors [4], but applications of the ghost imaging protocol (e.g. medical imaging, image cryptography) would be more practical with CCD imaging detectors and classical light.

In this paper, we use the solution of a wave transport equation describing the propagation of partially coherent light through a multiple-scattering medium to simulate near-field ghost images. We show that the presence of the residual ballistic component of the partially coherent field leads to the presence of a background in the image and the spatial resolution obtainable deteriorates with increasing size of the scattering elements relative to the wavelength.

2. Background

A schematic of a generic ghost imaging experiment is shown in figure 1. In the case of classical ghost imaging, an intense beam of partially coherent light is divided by a beam-splitter resulting in two beams of light, classically spatially correlated in both the near- and far-field [6, 10]. One

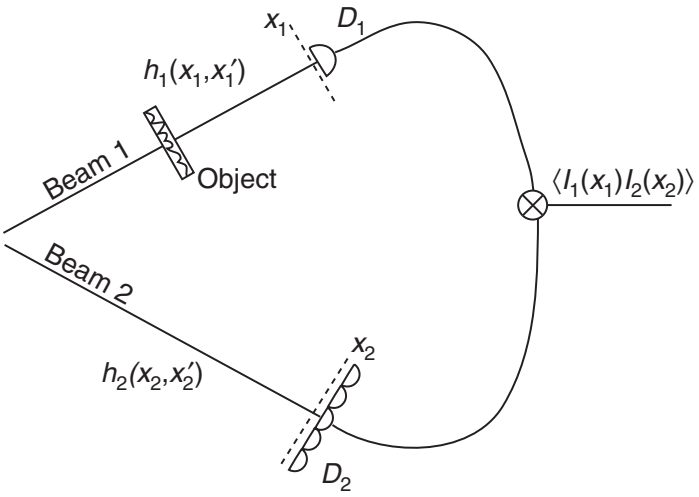

Figure 1. Schematic of a two-beam imaging experiment. The test arm corresponds to path 1 where the object is placed and a detector D_1 is used, while path 2 is the reference arm where a detector, D_2, possessing spatial resolution, is located.

beam is incident on the object to be imaged (the object or test beam), and the other propagates to a detector with spatial resolution (the reference beam). The function, in the one-dimensional case, describing the intensity fluctuation correlations $\Delta G(x_1, x_2)$ contains the image of the object [6] where [11, 12]:

$$\Delta G(x_1, x_2) = \langle I_1(x_1) I_2(x_2)\rangle - \langle I_1(x_1)\rangle\langle I_2(x_2)\rangle, \tag{1}$$

where I_1 and I_2 denote the intensities in the test and reference beams, respectively, x_1 and x_2 represent two points in the field and the brackets denote an average over all realisations of the field. As can be seen in (1), ΔG depends on the two intensities at the detectors, and thus is second order in intensity. It is also apparent that a background term, $\langle I_1(x_1)\rangle\langle I_2(x_2)\rangle$ must be subtracted from the pure intensity correlation term.

We consider here a partially coherent, quasi-monochromatic, scalar classical light source described by Gaussian statistics with zero mean [13]. As a consequence, the fourth-order correlation function can be expressed in terms of the second-order (field) spatial correlation function, $\Gamma(x_1, x_2)$ defined as

$$\Gamma(x_1, x_2) = \langle E^*(x_1) E(x_2)\rangle, \tag{2}$$

where E is the spatial field distribution of the source. In the case of classical two-beam imaging it can be shown [14] that ΔG is given by:

$$\Delta G(x_1, x_2) = \left| \int\int \Gamma(x_1', x_2') h_1(x_1', x_1) h_2^*(x_2', x_2)\, \mathrm{d}x_1\, \mathrm{d}x_2 \right|^2, \tag{3}$$

where h_1 and h_2 are the impulse response functions describing the optical paths of the test and reference beams, respectively [15]. It is apparent from (3) that the image obtained in classical

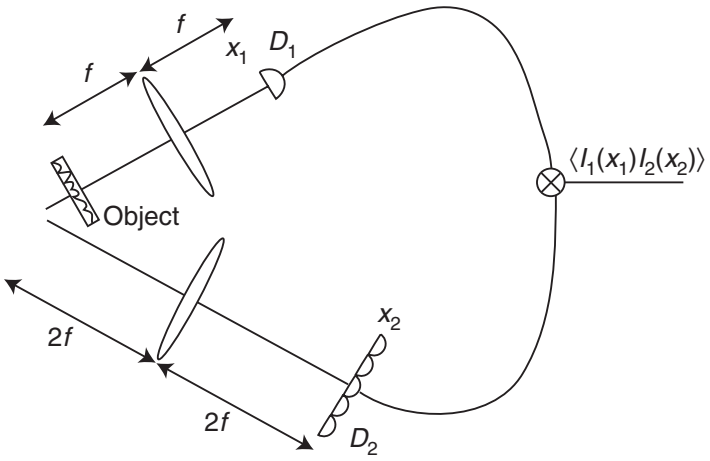

Figure 2. Particular arrangement for obtaining a near-field transmission image of an object with two-beam correlated imaging, where in arm 1 the object is very close to the source and a lens is used to collect the light in a bucket detector, while in arm 2 an imaging configuration is used.

ghost imaging is therefore critically dependent on the second-order correlation function, Γ, of the source.

Although the approach adopted is quite general, we here examine the influence on the resulting image in the specific case where the reference beam, shown in figure 2, is in the $2f$:$2f$ imaging configuration. The object is described by a complex transmission function $t(x)$. In this case it can be shown that [6]

$$\Delta G(x_1, x_2) \propto \left| \int \mathrm{d}x_1' \Gamma(x_1', -x_2) t^*(x_1') \exp\left(\frac{\mathrm{i}kx_1'x_1}{f}\right) \right|^2, \tag{4}$$

where λ is the wavelength of the source, $k = 2\pi/\lambda$ and f is the focal length of the lens. Ghost imaging experiments often determine the marginal intensity

$$I_\mathrm{m}(x_2) = \int \Delta G(x_1, x_2)\, \mathrm{d}x_1, \tag{5}$$

which is equivalent to having a 'bucket' detector in the test arm. It can easily be seen that if the correlation function, $\Gamma(x_1, x_2)$, is extremely narrow and can be approximated by $\delta(x_1 - x_2)$, then the marginal intensity will be approximately proportional to the magnitude squared of the transmission function, $|t(-x_2)|^2$, in the case of illumination with light of uniform intensity. The width of the correlation function corresponds to the spatial extent of correlations between two non-identical points in space, and is related to the coherence length of the source. In order to obtain an image of an object with high spatial resolution, Γ must be narrow; i.e. the coherence length of the light incident on the beam-splitter must be small. Simply stated, the smallest feature in the object must be approximately larger in size than the width of $\Gamma(x_1, x_2)$ [14].

When creating a pseudo-thermal source by passing a coherent beam through a turbid medium, the second-order correlation function of the pseudo-thermal light consists of the superposition of a broad coherent ballistic (unscattered) portion, and a narrow scattered component [16]. The relative fractions of ballistic and scattered components can be changed by altering the concentration and size of the particles in the turbid medium. Previous theoretical

simulations of classical ghost imaging using partially coherent light assumed a beam described by a Gaussian–Schell model [17], which does not permit an analysis of the influence on the resulting image of the properties of the scattering medium or the contribution from the residual ballistic component.

A number of methods can be used to calculate the second-order correlation function of scattered light [16], [18]–[20]. Here, we use the method proposed by Cheng and Raymer [16], based on a wave transport approach equivalent to using the extended Huygens–Fresnel principle in the small-angle scattering approximation [18]. Using this technique, it can be shown that after propagation through a medium with optical path length z, the spatial coherence function, $J(x, s, z) = \Gamma(x + s/2, x - s/2, z)$, where $s = x_1 - x_2$ and $x = (x_1 + x_2)/2$, can be written in the form

$$J(x, s, z) = \int \mathrm{d}q \exp[\mathrm{i}qx] \exp[-I_1(s, q, z)] I_0(s, q, z), \tag{6}$$

$$I_1(s, q, z) = \mu_t z - \frac{N\sigma\sqrt{\pi}}{\theta_0 q}\left\{\mathrm{erf}\left[\frac{k\theta_0}{2}s\right] - \mathrm{erf}\left[\frac{k\theta_0}{2}(s - qz/k)\right]\right\} \tag{7}$$

and

$$I_0(s, q, z) = \frac{1}{2\pi}\exp\left[-\frac{(s - qz/k)^2}{4a^2} - \frac{a^2q^2}{4}\right], \tag{8}$$

where a is the width of the incoming coherent, assumed Gaussian profile, laser source, N is the number concentration of scatterers, σ is the total scattering cross-section, θ_0 is the width of a Gaussian fitted to the differential scattering cross-section and μ_t is the extinction coefficient. These final three parameters can be obtained using Mie scattering theory [18]. Note that any absorption by the particles has been ignored in our simulations. The resulting correlation function can then be used in numerical simulations based on equation (3) to calculate the marginal intensity. Note that the spatial coherence function calculated using equation (6) refers to the field captured by the subsequent optical system. Since the aim of the simulations shown here is to highlight the salient features introduced by scattering, the effect of the finite numerical aperture of any real system is not included in any calculations shown here.

3. Correlation function

Figure 3 shows $\Gamma(x_1, x_2)$ for a Gaussian beam of $1/e$ width 2.12 mm that has passed through a 5 mm optical path length water/glycerol mixture containing 20 μm diameter polystyrene microspheres. A water/glycerol mixture is commonly used to achieve neutral buoyancy of polystyrene microspheres [21].

It can be seen that, in general, the correlation function consists of a superposition of a ballistic component which appears as a circular background and a scattered component which has a narrow distribution about the diagonal $x_1 = x_2$. Hence, as the strength of the scattered component relative to the residual unscattered field increases, $\Gamma(x_1, x_2)$ more closely approximates the narrow function required to produce ghost images in the configuration of figure 2. Any ballistic component still present in the beam as it leaves the scattering medium leads to a broad pedestal in $\Gamma(x_1, x_2)$ which would be expected to produce a low spatial resolution background in any ghost image. It is evident that the strength of the ballistic component will decrease by increasing the concentration or the size of the particles or increasing

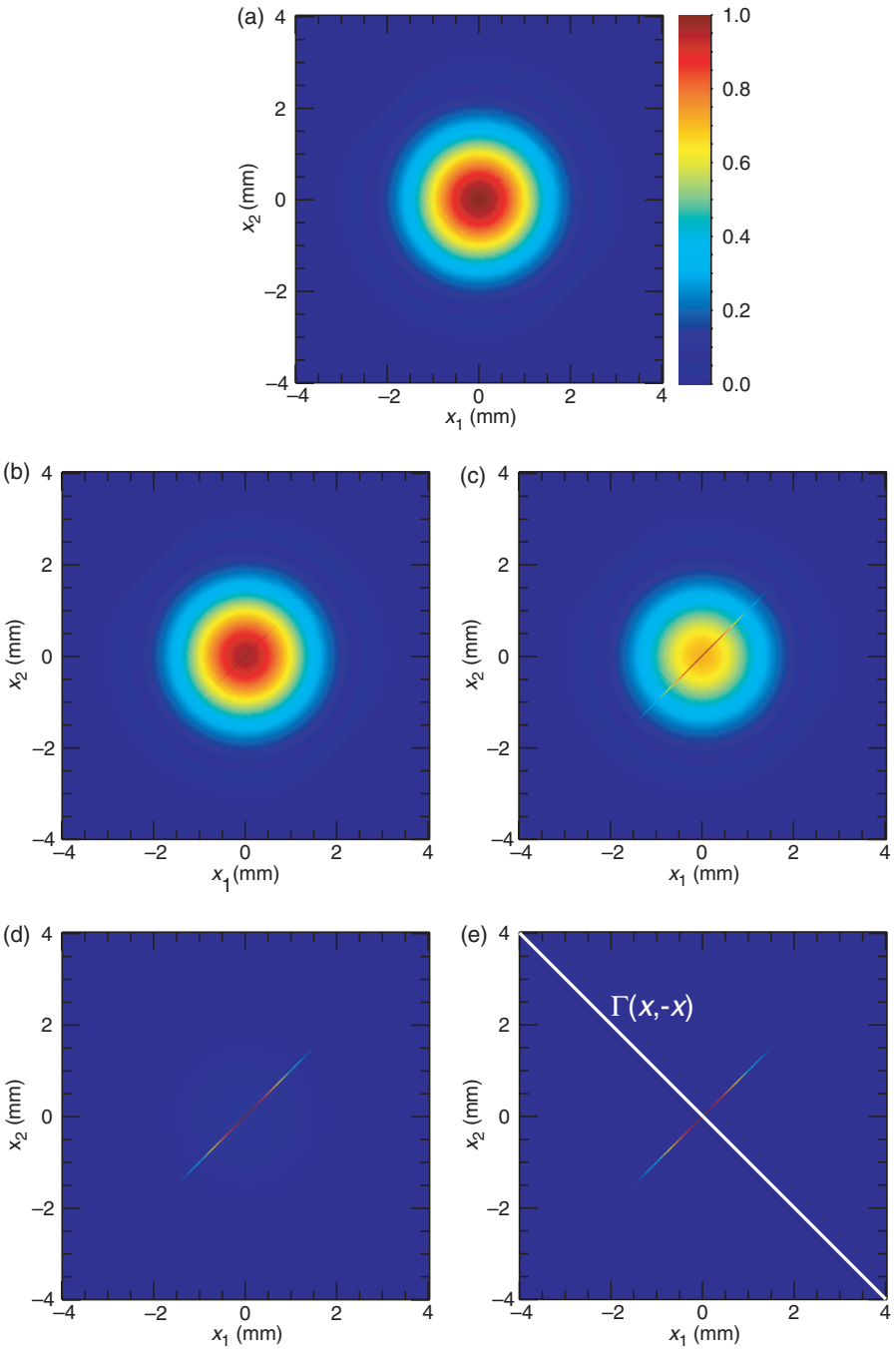

Figure 3. The normalised second-order correlation function, $\Gamma(x_1, x_2)$, of an initially spatially coherent Gaussian profile beam that has propagated through 5 mm of a medium of refractive index 1.60 containing different volume concentrations, N, of polystyrene microspheres of diameter 20 μm. The intensity $1/e$ full-width of the incident beam is 2.12 mm and the wavelength 633 nm. (a) No microspheres present, (b) $N = 10^{10}$ spheres m^{-3}, (c) $N = 10^{11}$ spheres m^{-3}, (d) $N = 10^{12}$ spheres m^{-3}, (e) $N = 10^{13}$ spheres m^{-3}. For each parameter set, $\Gamma(x_1, x_2)$ was normalised to its maximum value.

Table 1. The $1/e$ full-width of a Gaussian fitted to a diagonal line, $\Gamma(x, -x)$, through the second-order correlation function of light with a wavelength of 633 nm that has passed through a scattering medium of path length 5 mm containing polystyrene microspheres with a fixed OD of 5, but different diameters. The $1/e$ intensity width of the incident coherent beam is 2.12 mm. The error quoted is the 1-sigma error estimate.

Diameter (μm)	Width (μm)
5	2.92 ± 0.01
10	5.40 ± 0.03
20	10.83 ± 0.03
40	21.55 ± 0.06

the optical path length of the turbid medium. Hence, the extent of the suppression of the ballistic component is more appropriately characterized through the optical density, $\mathrm{OD} = N\sigma z$.

Although the width of the ballistic component changes only slightly with changes in the parameters describing the scattering medium, the width of the scattered component, which is critical to determining the spatial resolution obtainable with the resulting pseudo-thermal source, is a sensitive function of the particle size. Table 1 shows the width of the scattered component of $\Gamma(x, -x)$ (see figure 3(e)) for scattering media containing spheres of different diameters, but with a fixed OD of 5. It can be seen that as the particle size increases, the width of the scattered component also increases and is of the same order as the particle diameter. Further simulations (not shown here) also indicate that the width, $\Gamma(x, -x)$, is independent of the dimensions of the incident Gaussian beam. Implications for ghost imaging are discussed in the next section.

4. Imaging simulation

The results of our simulations show that there are two critical parameters in estimating the quality of a ghost image: the relative strength of the ballistic component compared to the scattered component and the coherence length of the scattered component. To investigate the influence that the properties of the scattering medium have on the marginal intensity of a ghost image, correlation functions computed using equation (6) were used to simulate the results for the imaging arrangement shown in figure 2. Images of an opaque mask containing two slits of width 150 μm and separated by 300 μm were calculated. A scattering medium of path length 5 mm and containing particles with diameters of 20 μm was used and the impact of changing the particle concentration on the marginal intensity is shown in figure 4.

It can be seen that the marginal intensity is a superposition of a broad background produced by the residual ballistic component and an image of the object (modulated by the intensity of the field) resulting from the low coherence scattered component. Note that the background is in addition to the intensity background that must be subtracted from the intensity correlations to determine ΔG in equation (1). The presence of a significant ballistic component permits imaging of objects with detail no smaller than approximately the diameter of the original coherent light source, so in this case, where the beam diameter is 2.12 mm, the ballistic portion

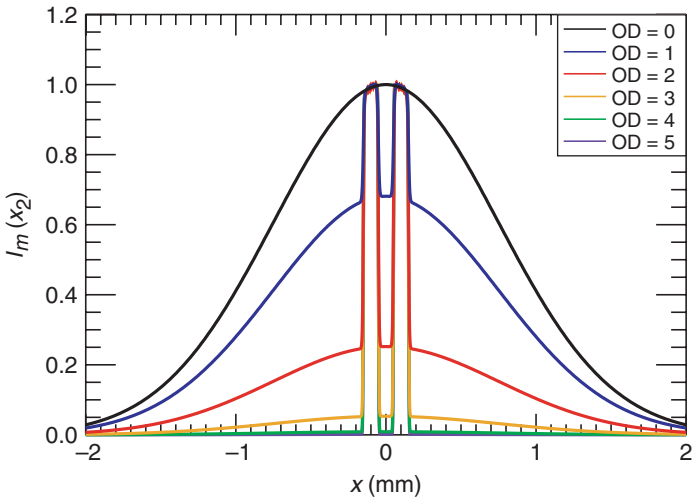

Figure 4. The normalised simulated marginal intensity showing a ghost image of an opaque mask containing two slits of width 100 μm separated by a distance of 200 μm. Imaging has been performed with light that has passed through a scattering medium containing 20 μm spheres with different ODs. The $1/e$ intensity width of the incident coherent beam is 2.12 mm and its wavelength is 633 nm.

of the light carries no object information. Figure 4 shows that the OD can be selected to reduce the ballistic contribution to an arbitrarily low level. Secondary methods, such as the inclusion of a rotating diffuser are also widely employed to eliminate any remaining unscattered component.

To demonstrate the effect that increasing the diameter of the scattering spheres has on the resolution of a ghost image, for a fixed OD of 5 and wavelength of 633 nm, the transmission function was changed to represent a double slit mask with a slit width of 20 μm and a slit separation of 30 μm. The results are shown in figure 5.

It is immediately clear from figure 5 that increasing the diameter of the scatterers, while keeping both the OD of the medium and the wavelength of the light fixed, leads to poorer spatial resolution in the ghost image. The larger diameter spheres create a more coherent scattered wave with a narrower differential scattering cross-section. As a consequence, the object becomes less well resolved as the sphere diameter increases. It has previously been shown [22] by a consideration of the near-field speckle size that the spatial resolution obtainable is of the order of magnitude of the particle size which is consistent with the results obtained here. Note that the key parameter determining the differential scattering cross-section, is the ratio of the particle diameter to the wavelength of the light used. Hence, it is anticipated that it is this parameter that will ultimately influence the spatial resolution. It should also be emphasised that our simulations show no influence of the incident beam size on the spatial resolution obtainable. Since perfect ensemble averaging is implicitly assumed in the use of the wave-transport approach, one of its limitations is that it provides no specific information about the obtainable image signal-to-noise ratio. Such issues are better addressed through a stochastic approach.

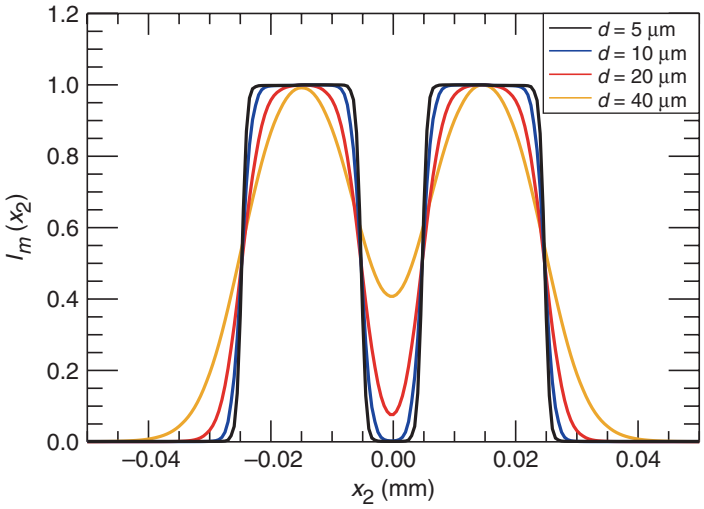

Figure 5. The normalised simulated marginal intensity showing a ghost image of a mask containing two slits of width 20 μm separated by a distance of 30 μm. Imaging has been performed with light that has passed through a scattering medium with a fixed OD of 5 containing spheres with different diameters. The wavelength is 633 nm.

5. Conclusion

The wave transport model used in this paper provides a means to predict the coherence of pseudo-thermal light created by passing initially coherent light through a scattering medium. The calculated coherence function can be used to simulate the results of classical two-beam ghost imaging experiments.

Two central conclusions can be drawn. Firstly, the presence of the residual ballistic component in the scattered wave-field leads to the presence of a low-resolution background in the marginal intensity. We have shown that increasing the OD of the scattering medium can reduce the influence of the ballistic component to an arbitrarily low level, although there are a number of secondary means that could also be used to reduce its strength. Secondly, for a fixed wavelength, the spatial coherence length of the scattered component of the field increases with increasing sphere diameter, leading to a deterioration in the spatial resolution obtainable in the resulting ghost image. More generally, the spatial resolution will be determined by the ratio of the particle size to the wavelength of light used.

Acknowledgments

This research was supported under the Australian Research Council Discovery Projects funding scheme (project number DP0557505) and S Crosby acknowledges the receipt of an Australian Postgraduate Award.

References

[1] Pittman T B, Shih Y H, Strekalov D V and Sergienko A V 1995 *Phys. Rev.* A **52** R3429
[2] Saleh B E A, Abouraddy A F, Sergienko A V and Teich M C 2000 *Phys. Rev.* A **62** 043816
[3] Abouraddy A F, Saleh B E A, Sergienko A V and Teich M C 2002 *J. Opt. Soc. Am.* B **19** 1174
[4] Valencia A, Scarcelli G, D'Angelo M and Shih Y H 2005 *Phys. Rev. Lett.* **94** 063601
[5] Zhang D, Zhai Y H, Wu L A and Chen X H 2005 *Opt. Lett.* **30** 2354
[6] Ferri F, Magatti D, Gatti A, Bache M, Brambilla E and Lugiato L A 2005 *Phys. Rev. Lett.* **94** 183602
[7] D'Angelo M and Shih Y H 2005 *Laser Phys. Lett.* **2** 567 and references therein
[8] D'Angelo M, Valencia A, Rubin M H and Shih Y 2005 *Phys. Rev.* A **72** 013810
[9] Abouraddy A F, Saleh B E A, Sergienko A V and Teich M C 2001 *Phys. Rev. Lett.* **87** 123602
[10] Gatti A, Bache M, Magatti D, Brambilla E, Ferri F and Lugiato L A 2006 *J. Mod. Opt.* **53** 739
[11] Gatti A, Brambilla E and Lugiato L A 2003 *Phys. Rev. Lett.* **90** 133603
[12] Gatti A, Brambilla E, Bache M and Lugiato L A 2004 *Phys. Rev. Lett.* **93** 093602
[13] Mandel L and Wolf E 1995 *Optical Coherence and Quantum Optics* (Cambridge: Cambridge University Press)
[14] Gatti A, Brambilla E, Bache M and Lugiato L A 2004 *Phys. Rev.* A **70** 013802
[15] Goodman J W 1968 *Fourier Optics* (New York: McGraw-Hill)
[16] Cheng C and Raymer M G 2000 *Phys. Rev.* A **62** 023811
[17] Cai Y and Zhu S 2004 *Opt. Lett.* **29** 2716
[18] Henyey L and Greenstein J 1941 *Astrophys. J.* **93** 70
[19] Shipley S and Weinman J 1978 *J. Opt. Soc. Am.* **68** 130
[20] Luebbers R and Hunsberger H 1992 *IEEE Trans. Antennas Propag.* **40** 1297
[21] Wax A and Thomas J E 1998 *J. Opt. Soc. Am.* A **15** 1896
[22] Bache M, Magatti D, Ferri F, Gatti A, Brambilla E and Lugiato LA 2006 *Phys. Rev.* A **73** 053802